

Quantum spin Hall phase in GeSn heterostructures on silicon

B. M. Ferrari¹, F. Marcantonio¹, F. Murphy-Armando², M. Virgilio³ and F. Pezzoli^{1,*}¹Dipartimento di Scienza dei Materiali, Università di Milano-Bicocca, LNESS and BiQuTe, via Cozzi 55, 20125 Milano, Italy²Tyndall National Institute, Cork T12R5CP, Ireland³Dipartimento di Fisica, Università di Pisa, Largo Pontecorvo 3, I-56127 Pisa, Italy

(Received 3 August 2022; accepted 19 April 2023; published 22 May 2023)

Quantum phases of solid-state electron systems can sustain exotic phenomena and a very rich spin physics. We utilize model-solid theory to show that $\text{Ge}_{1-x}\text{Sn}_x$ alloys, an emerging group IV semiconductor, can be engineered into heterostructures that demonstrate a broken-gap alignment. Furthermore, the eight-band $k \cdot p$ method is used to disclose a quantum spin Hall phase in heterojunctions that accommodates the existence of gate-controlled chiral edge states. This proposal introduces a practical silicon-based architecture that spontaneously sustains topological properties, while being compatible with the high-volume manufacture of semiconductor technologies.

DOI: [10.1103/PhysRevResearch.5.L022035](https://doi.org/10.1103/PhysRevResearch.5.L022035)

The hybridization between valence and conduction states at surfaces and interfaces has been recognized as a key-enabling solution for the realization of topological protected states [1–4]. In heterostructures possessing a broken-gap (BG) alignment of the band edges, electron and hole subbands can be localized at opposite sides of the junctions, while simultaneously retaining the inverted ordering regime [3]. This leads to the emergence of helical boundary states, which are characteristic fingerprints of the so-called quantum spin Hall (QSH) phase [1,2,5–10]. Challenges, however, remain before these concepts can be harnessed for their practical use. Were QSH capabilities realized in group IV materials, this would bring exceptional topological properties into mass-produced devices. Yet, the crucial BG band lineup is the missing ingredient that presently hampers the achievement of genuine quantum phases in such systems.

In this Letter we introduce group IV architectures that will enable quantum phase transitions in ubiquitous Si-based devices. We leverage model-solid theory [11] and demonstrate an unexpected BG in heterojunctions based on $\text{Ge}_{1-x}\text{Sn}_x$. This enables the previously unexplored capacity of group IV systems to sustain the coveted QSH phase as we will show in specific $\text{Ge}_{1-x}\text{Sn}_x/\text{Ge}_{1-y}\text{Sn}_y$ superlattices (SL) by multiband $k \cdot p$ calculations. We show that strain and quantum confinement offer practical degrees of freedom to engineer the topological phase transitions. Finally, we extend our investigation to finite-size SLs connected to gate leads using self-consistent modeling. We explore realistic device geometries and validate the addition of the electrical tunability

owned by topological architectures that harbor the unprecedented potential of being monolithically integrated on Si substrates.

Lately, alloying Ge with Sn has attracted attention because it provides a means to induce a transition of the fundamental energy gap [12–15]. Present-day epitaxy of $\text{Ge}_{1-x}\text{Sn}_x$ on Si is well established and industrial techniques have already succeeded in synthesizing materials with Sn contents above 30 at. % [16,17]. Here we envision an heteroepitaxial stack grown on the so-called virtual substrate (VS), which accommodates the mismatch between the lattice parameters ($a_{\text{Sn}} > a_{\text{Ge}} > a_{\text{Si}}$) and consists of a $\text{Ge}_{1-s}\text{Sn}_s$ buffer deposited on a common Si(100) wafer. Henceforth, the growth axis k is assumed along [100]. The topmost VS film is a relaxed alloy, which can then be used as a template for the repeated deposition of $\text{Ge}_{1-x}\text{Sn}_x/\text{Ge}_{1-y}\text{Sn}_y$ bilayers in a state of biaxial tension or compression, owing to the lattice mismatch with the selected VS. The most feasible method to fabricate VSs would be a standard compositionally graded film [18–20], but other strategies have been also shown to be accessible [21]. Experimental efforts have also demonstrated that the deposition under strain-unbalanced conditions and the growth of SL with repeated discontinuities in the Sn content are possible [22–24].

To disclose a rational design of QSH insulators on Si we begin by considering the band alignment established at the $\text{Ge}_{1-x}\text{Sn}_x/\text{Ge}_{1-y}\text{Sn}_y$ heterointerface. We assume the films to be in full registry with the lattice of a fully relaxed $\text{Ge}_{1-s}\text{Sn}_s$ buffer. To minimize the computational burden, we rely on the flexible approach offered by the model-solid theory that enable us to compute interface lineups by including strain effects [11]. The parameters and validation of the model are provided in Ref. [25]. Another important point is that we focus on strained films that are predicted to have a direct band gap. This can provide a viable solution to avoid the competitive presence of absolute minima at the zone edges, like the characteristic L-valleys in relaxed Ge, that

*fabio.pezzoli@unimib.it

Published by the American Physical Society under the terms of the [Creative Commons Attribution 4.0 International](https://creativecommons.org/licenses/by/4.0/) license. Further distribution of this work must maintain attribution to the author(s) and the published article's title, journal citation, and DOI.

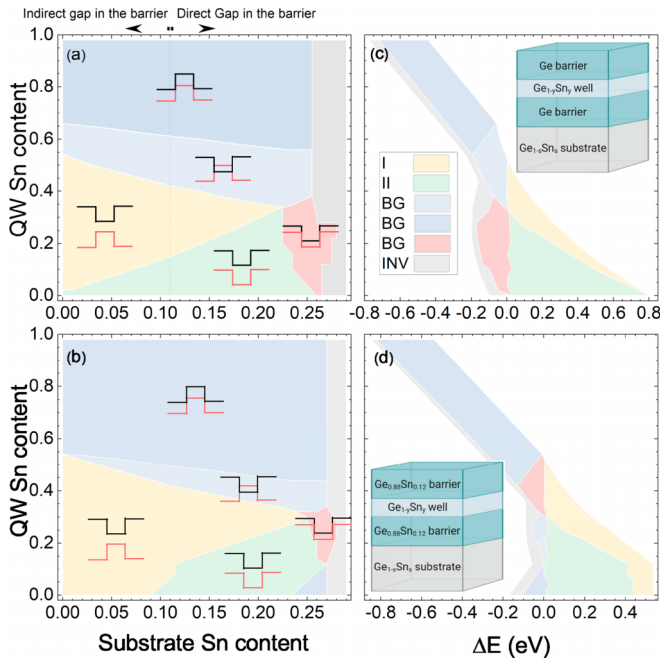


FIG. 1. Band edges of $\text{Ge}/\text{Ge}_{1-y}\text{Sn}_y/\text{Ge}$ (a) and $\text{Ge}_{0.88}\text{Sn}_{0.12}/\text{Ge}_{1-y}\text{Sn}_y/\text{Ge}_{0.88}\text{Sn}_{0.12}$ (b) heterojunctions as a function of the Sn concentration of the relaxed substrate. The well/barrier stack is coherent with the $\text{Ge}_{1-y}\text{Sn}_y$ lattice. The schematics demonstrate type I (yellow), type II (green), and broken-gap (BG, red, light blue, and dark blue) alignments. The region where the band inversion occurs within the same layer as in bulk topological materials is also shown (INV, gray). In panel (b), the barriers feature a direct gap regardless of the Sn content of the substrate. The minimum energy differences (ΔE) between conduction and valence bands across $\text{Ge}/\text{Ge}_{1-y}\text{Sn}_y/\text{Ge}$ (c) and $\text{Ge}_{0.88}\text{Sn}_{0.12}/\text{Ge}_{1-y}\text{Sn}_y/\text{Ge}_{0.88}\text{Sn}_{0.12}$ (d) are also shown. Schematics of the heterostructures (not to scale) are shown as insets.

could impede the observation of the QSH phase in future experiments.

For consistency with the literature, we consider a symmetric $\text{Ge}_{1-x}\text{Sn}_x/\text{Ge}_{1-y}\text{Sn}_y/\text{Ge}_{1-x}\text{Sn}_x$ heterostructure. Without loss of generality, the two external identical $\text{Ge}_{1-x}\text{Sn}_x$ films are dubbed “barriers,” whereas the intermediate $\text{Ge}_{1-y}\text{Sn}_y$ layer is termed “well.” The lineups at the heterointerface have been obtained by varying the strain in the epitaxial stack through the modification of the Sn molar fraction of the $\text{Ge}_{1-y}\text{Sn}_y$ buffer. We utilized elemental Ge and a $\text{Ge}_{0.70}\text{Sn}_{0.30}$ alloy. The latter has been chosen as an upper limit to guarantee experimental feasibility using state-of-the-art deposition techniques. For the same reason, we restricted the barriers to a Sn-diluted regime, namely, $x < 12\%$. Even though in this work we focus on the experimentally accessible region of the parameter space, the $\text{Ge}_{1-y}\text{Sn}_y$ well was allowed to freely sample the whole composition range ($0 < y < 1$) to give a better overview of all the domains potentially characterized by the sought-after BG. Figure 1 summarizes the results that were obtained when opposite ends of the y range were considered [25]. As a guideline, Figures 1(a) and 1(b) also report a schematic of the offsets at the conduction band (black lines) and at the top of the valence band (red lines). The strain

dependence is shown in Fig. S3 of Ref. [25]. Its comparison with the degree of strain relaxation presently achievable in epitaxial VSs [20] demonstrates that the residual compressive strain in the substrate has a negligible impact on the final band alignment.

It is interesting to notice the rich atlas of lineups unleashed in the $\text{Ge}_{1-x}\text{Sn}_x$ system. Insights can be obtained by the gross features that exquisitely appear in Figs. 1(a) and 1(b). When the Sn molar fraction of the substrate is higher than ~ 0.26 , a Sn bulklike band structure can be achieved within the films [INV, gray in Figs. 1(a) and 1(b)]. However, when $s < 0.26$, an inverted regime can be prominently observed when the Sn content of the $\text{Ge}_{1-y}\text{Sn}_y$ wells exceeds $\sim 50\%$. Specifically, a region exhibiting an inverted type-I feature, as in HgTe/CdTe , opens below 60%, while a distinct InAs/GaSb -like BG develops well above 60% [Fig. 1(a)]. At a first glance, $\text{Ge}_{1-y}\text{Sn}_y$ wells with a Sn molar fraction larger than 50% can be regarded as strong candidates for hosting topologically nontrivial phases. It should be noticed that, although very promising, alloys of high Sn content are hard to synthesize. In the low Sn content scenario, namely, when $\text{Ge}_{1-y}\text{Sn}_y$ wells with $y < 0.5$ are considered, the strain imprinted by the substrate appears to restore the normal band sorting, featuring either a type-I (yellow area) or a staggered type-II (green area) alignment [Fig. 1(a)]. In the latter case, charges are set apart at opposite sides of the heterointerface, where a well-defined insulating gap is retained. Surprisingly, in this diluted alloy regime there exists a region in which our calculations predict the emergence of a unique BG. This occurs around $0.23 < s < 0.3$ and $0 < y < 0.4$ and is marked in red in Figs. 1(a) and 1(b). Such a domain has the advantage of having a direct gap in both the well and the substrate at compositions where band mixing effects are negligible [26,27] and of being manifested in heterostructures that are easier to grow through epitaxial techniques. Another central finding regarding the interface alignments is the energy difference ΔE calculated between the bottommost conduction band edges and the topmost valence band, which is established across the junction. Figures 1(c) and 1(d) demonstrate negative (positive) ΔE when the inverted (normal) band ordering sets in. Interestingly, ΔE can be extraordinarily large as these gaps possess remarkable amplitudes in the range of several hundreds of meV. This offers indeed plausible prospects for topological applications above cryogenic temperatures.

In the following we turn our attention to a $\text{Ge}_{0.88}\text{Sn}_{0.12}/\text{Ge}_{0.78}\text{Sn}_{0.22}$ multilayer stack and analyze the evolution of the electronic states as a function of the thickness of the layers as well as the strain relative to the substrate. In Fig. 1 such an heterointerface lays within the parameter space previously disclosed by the model-solid theory as the source of a BG.

We now leverage a multiband $k \cdot p$ model [28] to unveil the richness in terms of quantum phases and to fully capture the essential physics of this intriguing $\text{Ge}_{1-x}\text{Sn}_x$ platform. For a discussion of the parametrization, see Ref. [25]. At first, we investigate an infinite periodic $\text{Ge}_{0.88}\text{Sn}_{0.12}/\text{Ge}_{0.78}\text{Sn}_{0.22}$ SL. We set the thickness of the $\text{Ge}_{0.78}\text{Sn}_{0.22}$ well at 10 nm, while the width of the $\text{Ge}_{0.88}\text{Sn}_{0.12}$ barrier is maintained relatively large, e.g., 25 nm, to ensure a reduced penetration of the wave functions throughout the whole SL period. The energy

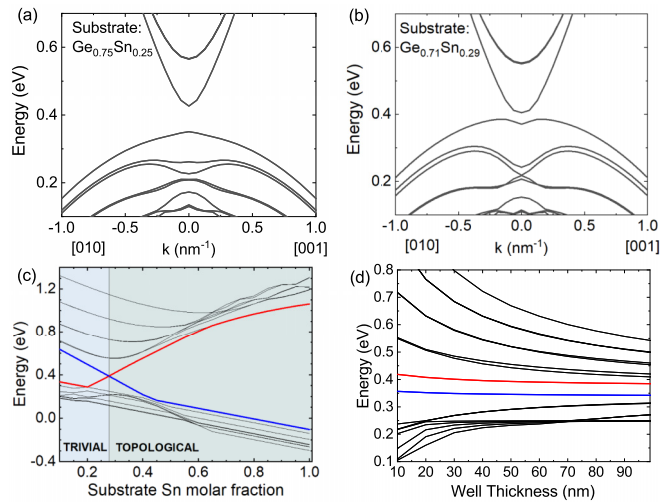


FIG. 2. In-plane dispersion calculated in a $\text{Ge}_{0.78}\text{Sn}_{0.22}$ (10 nm)/ $\text{Ge}_{0.88}\text{Sn}_{0.12}$ (25 nm) superlattice (SL) coherently grown on relaxed $\text{Ge}_{0.75}\text{Sn}_{0.25}$ (a) and $\text{Ge}_{0.71}\text{Sn}_{0.29}$ (b). (c) Energy levels of a 10-nm $\text{Ge}_{0.78}\text{Sn}_{0.22}$ quantum well (QW) embedded in $\text{Ge}_{0.88}\text{Sn}_{0.12}$ barriers of 25 nm as a function of the Sn molar fraction of the $\text{Ge}_{1-s}\text{Sn}_s$ template. The lowest subband energies for the heavy-hole and electronlike states are indicated as red and blue lines, respectively. (d) Energy of the states of a $\text{Ge}_{0.78}\text{Sn}_{0.22}$ QW embedded in $\text{Ge}_{0.88}\text{Sn}_{0.12}$ barriers as a function of the well thickness. The substrate is a relaxed $\text{Ge}_{0.7}\text{Sn}_{0.3}$.

spectra calculated by the exact diagonalization of the $k \cdot p$ model shows the expected miniband features for the out-of-plane momentum (Fig. S6 of Ref. [25]). Whereas when the virtual substrate terminates with $\text{Ge}_{0.75}\text{Sn}_{0.25}$ [Fig. 2(a)] and $\text{Ge}_{0.71}\text{Sn}_{0.29}$ [Fig. 2(b)], the dispersion along the well plane suggests strain to be a pivotal driving force for the closure of the band gap and the likely cause of the hybridization between electron and hole states. Figure 2(c) summarizes the calculated shift of the energy levels of the SL as a function of the Sn content of the buffer. A striking transition from a trivial to a topological insulator can be clearly seen to occur at the critical value $s_c = 0.27$. The strain introduced by the substrate provokes indeed an opposite behavior for the electron and hole subbands, yielding a crossover that drives the SL structure into an inverted scheme when $s > s_c$ [Fig. 2(c)]. Notice that in the topological regime, that is, above s_c , the opening of the bulk insulating gap can be tuned in a very drastic way, as it remarkably approaches a magnitude of more than 1 eV in the limiting, although unpractical, case of growth on almost pure Sn buffers. We can find reassurance on these results by the agreement with the ΔE band offsets disclosed by the model-solid theory. Remarkably, the amplitude of the gapped bulk of our $\text{Ge}_{1-x}\text{Sn}_x$ proposal is exceedingly large compared to conventional two-dimensional (2D) QSH insulators, whose value typically lays below 10 meV [1,3,7,8], and compares well with atomically thin materials [10].

Next, we consider a $\text{Ge}_{0.7}\text{Sn}_{0.3}$ buffer whose Sn content is above s_c . Figure 2(d) shows no crossing points in the investigated range of the well thickness, thereby indicating that width fluctuations cannot destroy the attained normal and nontrivial insulator regimes. In the following, we focus on

the study of the edge state spectrum to explicitly demonstrate the emergence of the gapless helical states. To achieve this purpose, we set an equal thickness of 25 nm for both the well and the barrier layers and break the translational symmetry of the SL by opening free surfaces along the crystallographic direction $j \parallel [010]$ lying in the QW plane, while keeping periodic boundary conditions along k as shown in Fig. 3(a). The lateral dimension of the nanoribbon along j is set to 300 nm to minimize interactions between states laying at opposite facets of the Hall bar [Fig. 3(a)]. In Fig. 3(b) we report the electronic band structure in the neighbor of the Γ point along the i direction chosen parallel to the $[001]$ crystallographic axis. Figure 3(b) shows two linearly dispersing energy states (red) appearing inside of the gapped bulk (black) and crossing each other at the Γ point. Figure 3(c) reports the square modulus of the wave function associated with these states, which are confined along the growth axis k and behave as plane wave in the i direction, which is in the SL plane. Above all, their vanishing square amplitude in the bulk of the SL, that is, along j , openly unveils that these are Kramers pairs tightly localized at the opposite sides of the nanoribbon (see also Fig. S7 of the Ref. [25]). This eventually provides a compelling proof that the QSH phase indeed exists in group IV heterostructures. Calculations suggest that degenerate bulk states can possibly occur in these heterostructures, thus indicating that, as for bulk HgTe and α -Sn, special care will be needed to single out chiral edge states in future experimental works [29].

The unique coexistence and concomitant spatial separation of 2D electron and hole gases in the $\text{Ge}_{0.88}\text{Sn}_{0.12}/\text{Ge}_{0.78}\text{Sn}_{0.22}$ QSH insulator spontaneously establishes a dipole layer across the interface. This raises the attractive prospect of controlling the hybridization through electric fields. We discuss this possibility by focusing on the model $\text{Ge}_{0.88}\text{Sn}_{0.12}$ (25 nm)/ $\text{Ge}_{0.78}\text{Sn}_{0.22}$ (25 nm) SL in the form of a finite-size stack comprising ten periods, which we have studied for different Sn concentrations covering the range where a phase transition can occur. This allows us to identify, via self-consistent $k \cdot p$ calculations, the impact on the QSH phase of an external electrical bias, as we applied ohmic contacts at the two ends of the SL right along the k growth axis.

As we scan the Sn molar fraction of the substrate at zero bias, we recover the opening of a minigap within the valence band with the distinct formation of two complementary localized conductive edge states that become more pronounced as the Sn content, i.e., the strain, increases (see also Fig. S8 of Ref. [25] and Ref. [30]). The resulting density distribution further supports our conclusions as we find these states to be confined at the top and bottom surfaces when $s > 0.2$. It is worth noting that in this calculation the topological states emerge because of the finite dimension of the SL along the growth direction. That is distinct from the results obtained for the previously discussed infinite SL in the nanoribbon geometry (Fig. 3), thereby reinforcing the case for $\text{Ge}_{1-x}\text{Sn}_x$ -based heterostructures as robust hosts of the QSH phase. We therefore study the influence of an external bias on the topological structure, focusing on a strained SL deposited on a $\text{Ge}_{0.75}\text{Sn}_{0.25}$ buffer layer (see the device layout in Ref. [25]). The results are summarized in Fig. 4. Charge confinement manifests itself at 0 bias as a bending in a neighborhood

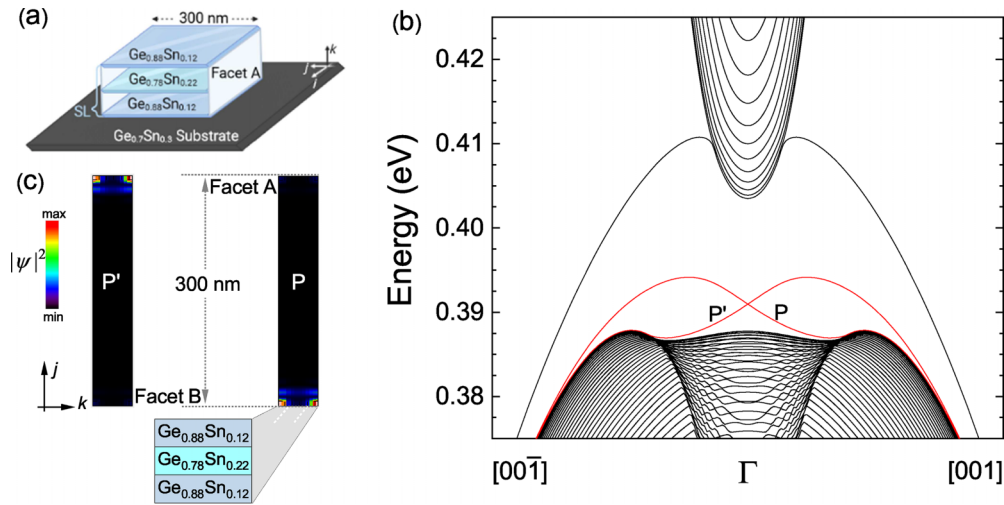


FIG. 3. (a) Schematics of a $\text{Ge}_{0.78}\text{Sn}_{0.22}(25 \text{ nm})/\text{Ge}_{0.88}\text{Sn}_{0.12}(25 \text{ nm})$ SL strained by a $\text{Ge}_{0.7}\text{Sn}_{0.3}$ substrate. The Hall bar has a width of 300 nm along j , i.e., the $[010]$ direction (not to scale). (b) Energy spectrum of the 2D ribbon along $i \parallel [001]$. The red lines highlight the topological states. (c) Color-coded maps showing the probability density $|\Psi|^2$ associated with the surface states (P and P').

of the final layers of the SL, while the profile at the center remains flat.

By applying a gentle positive bias, the edge states are more tightly confined and even more peaked at the free surfaces. At the same time, the external electric field drives the accumulation of charge density at each well/barrier interface as demonstrated by the characteristic bending profile, which is seemingly different from the flat band condition. Notably, the further increase of the polarization causes the edge states to

fade away [Figs. 4(c) and 4(f)], inducing a phase transition of the SL from a QSH to a trivial insulator. A finding that provides a novel route towards the implementation of topological field effect devices.

In conclusion, we unveiled quantum phases in Si-compatible materials beyond conventional systems. Our platform permits strain and electric field control of spin-orbit interaction [31–34] and quantum phases on Si. This concept is highly flexible and can have a longstanding

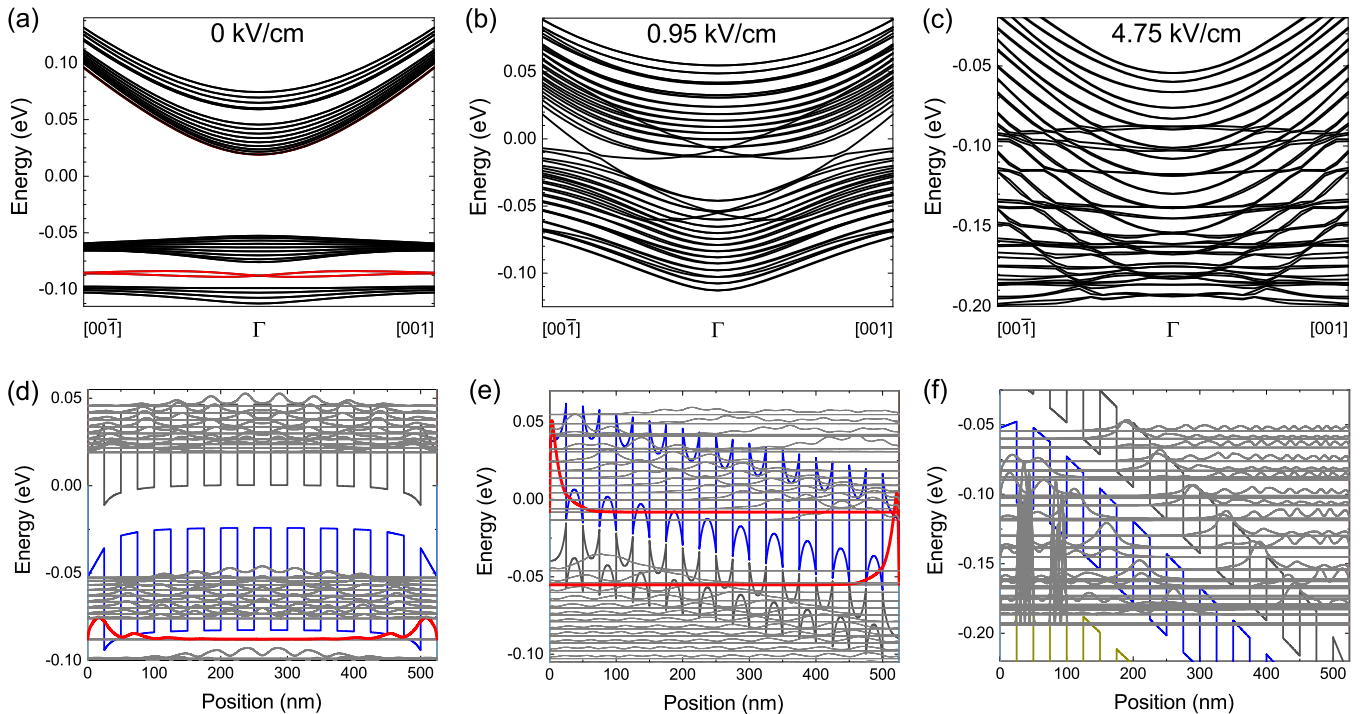


FIG. 4. Energy spectrum of a tenfold $\text{Ge}_{0.88}\text{Sn}_{0.12}(25 \text{ nm})/\text{Ge}_{0.78}\text{Sn}_{0.22}(25 \text{ nm})$ SL grown on $\text{Ge}_{0.75}\text{Sn}_{0.25}$. A scheme of the device is given in Ref. [25]. The SL is unbiased (a) or under an electric field of 0.95 kV/cm (b) or 4.75 kV/cm (c). The red branches indicate the topological states (see also Ref. [25]). Band edges and squared wave functions at the center of the Brillouin zone in an unbiased device (d) or when electric fields of 0.95 kV/cm (e) or 4.75 kV/cm (f) are applied.

impact, stimulating new research directions towards Si topology.

We acknowledge C. Colombo and A. Filippi for technical assistance with model-solid theory and $k \cdot p$ calculations,

respectively. This material is based upon work supported by the Air Force Office of Scientific Research under Award No. FA8655-22-1-7050. F.M.-A. would like to acknowledge Science Foundation Ireland Grant No. SFI/19/FFP/6953.

-
- [1] B. A. Bernevig, T. L. Hughes, and S.-C. Zhang, Quantum spin Hall effect and topological phase transition in HgTe quantum wells, *Science* **314**, 1757 (2006).
- [2] M. König, S. Wiedmann, C. Brüne, A. Roth, H. Buhmann, L. W. Molenkamp, X.-L. Qi, and S.-C. Zhang, Quantum spin hall insulator state in HgTe quantum wells, *Science* **318**, 766 (2007).
- [3] C. Liu, T. L. Hughes, X.-L. Qi, K. Wang, and S.-C. Zhang, Quantum Spin Hall Effect in Inverted Type-II Semiconductors, *Phys. Rev. Lett.* **100**, 236601 (2008).
- [4] M. Z. Hasan and C. L. Kane, Colloquium: Topological insulators, *Rev. Mod. Phys.* **82**, 3045 (2010).
- [5] I. Knez, R.-R. Du, and G. Sullivan, Evidence for Helical Edge Modes in Inverted InAs/GaSb Quantum Wells, *Phys. Rev. Lett.* **107**, 136603 (2011).
- [6] L. Du, I. Knez, G. Sullivan, and R.-R. Du, Robust Helical Edge Transport in Gated InAs/GaSb Bilayers, *Phys. Rev. Lett.* **114**, 096802 (2015).
- [7] M. S. Miao, Q. Yan, C. G. Van de Walle, W. K. Lou, L. L. Li, and K. Chang, Polarization-Driven Topological Insulator Transition in a GaN/InN/GaN Quantum Well, *Phys. Rev. Lett.* **109**, 186803 (2012).
- [8] D. Zhang, W. Lou, M. Miao, S.-c. Zhang, and K. Chang, Interface-Induced Topological Insulator Transition in GaAs/Ge/GaAs Quantum Wells, *Phys. Rev. Lett.* **111**, 156402 (2013).
- [9] Y. Xu, B. Yan, H.-J. Zhang, J. Wang, G. Xu, P. Tang, W. Duan, and S.-C. Zhang, Large-Gap Quantum Spin Hall Insulators in Tin Films, *Phys. Rev. Lett.* **111**, 136804 (2013).
- [10] M. S. Lodge, S. A. Yang, S. Mukherjee, and B. Weber, Atomically thin quantum spin Hall insulators, *Adv. Mater.* **33**, 2008029 (2021).
- [11] C. G. Van de Walle, Band lineups and deformation potentials in the model-solid theory, *Phys. Rev. B* **39**, 1871 (1989).
- [12] R. A. Soref and L. Friedman, Direct-gap Ge/GeSn/Si and GeSn/Ge/Si heterostructures, *Superlattices Microstruct.* **14**, 189 (1993).
- [13] G.-E. Chang, S.-W. Chang, and S. L. Chuang, Strain-balanced $\text{Ge}_z\text{Sn}_{1-z}-\text{Si}_x\text{Ge}_y\text{Sn}_{1-x-y}$ multiple-quantum-well lasers, *IEEE J. Quantum Elect.* **46**, 1813 (2010).
- [14] H. S. Maczko, R. Kudrawiec, and M. Gladysiewicz, Material gain engineering in GeSn/Ge quantum wells integrated with an Si platform, *Sci. Rep.* **6**, 34082 (2016).
- [15] S. Wirths, D. Buca, and S. Mantl, Si-Ge-Sn alloys: From growth to applications, *Prog. Cryst. Growth Ch.* **62**, 1 (2016).
- [16] C. Xu, D. Ringwala, D. Wang, L. Liu, C. D. Poweleit, S. L. Y. Chang, H. L. Zhuang, J. Menéndez, and J. Kouvetakis, Synthesis and fundamental studies of Si-compatible (Si)GeSn and GeSn mid-IR systems with ultrahigh Sn contents, *Chem. Mater.* **31**, 9831 (2019).
- [17] J. Zheng, Z. Liu, Y. Zhang, Y. Zuo, C. Li, C. Xue, B. Cheng, and Q. Wang, Growth of high-Sn content (28%) GeSn alloy films by sputtering epitaxy, *J. Cryst. Growth* **492**, 29 (2018).
- [18] W. Dou, Y. Zhou, J. Margetis, S. A. Ghetmiri, S. Al-Kabi, W. Du, J. Liu, G. Sun, R. A. Soref, J. Tolle, B. Li, M. Mortazavi, and S.-Q. Yu, Optically pumped lasing at 3 μm from compositionally graded GeSn with tin up to 22.3%, *Opt. Lett.* **43**, 4558 (2018).
- [19] W. Dou, M. Benamara, A. Mosleh, J. Margetis, P. Grant, Y. Zhou, S. Al-Kabi, W. Du, J. Tolle, B. Li, M. Mortazavi, and S.-Q. Yu, Investigation of GeSn strain relaxation and spontaneous composition gradient for low-defect and high-Sn alloy growth, *Sci. Rep.* **8**, 5640 (2018).
- [20] X. Liu, J. Zheng, M. Li, F. Wan, C. Niu, Z. Liu, Y. Zuo, C. Xue, and B. Cheng, Growth of relaxed GeSn film with high Sn content via Sn component-grade buffer layer structure, *J. Phys. D: Appl. Phys.* **54**, 435101 (2021).
- [21] S. Assali, J. Nicolas, and O. Moutanabbir, Enhanced Sn incorporation in GeSn epitaxial semiconductors via strain relaxation, *J. Appl. Phys.* **125**, 025304 (2019).
- [22] J.-Z. Chen, H. Li, H. H. Cheng, and G.-E. Chang, Structural and optical characteristics of $\text{Ge}_{1-x}\text{Sn}_x/\text{Ge}$ superlattices grown on Ge-buffered Si(001) wafers, *Opt. Mater. Express* **4**, 1178 (2014).
- [23] I. A. Fischer, C. J. Clausen, D. Schwarz, P. Zaumseil, G. Capellini, M. Virgilio, M. C. da Silva Figueira, S. Birner, S. Koelling, P. M. Koenraad, M. R. S. Huang, C. T. Koch, T. Wendav, K. Busch, and J. Schulze, Composition analysis and transition energies of ultrathin Sn-rich GeSn quantum wells, *Phys. Rev. Mater.* **4**, 024601 (2020).
- [24] M. Montanari, M. Virgilio, C. L. Manganelli, P. Zaumseil, M. H. Zoellner, Y. Hou, M. A. Schubert, L. Persichetti, L. Di Gaspare, M. De Seta, E. Vitiello, E. Bonera, F. Pezzoli, and G. Capellini, Photoluminescence study of interband transitions in few-layer, pseudomorphic, and strain-unbalanced Ge/GeSi multiple quantum wells, *Phys. Rev. B* **98**, 195310 (2018).
- [25] See Supplemental Material at <http://link.aps.org/supplemental/10.1103/PhysRevResearch.5.L022035> for more details on the numerical simulations, the dependence of the band-edge alignments on strain and Sn content, and the energy spectrum of finite-sized unbiased superlattices.
- [26] E. J. O'Halloran, C. A. Broderick, D. S. P. Tanner, S. Schulz, and E. P. O'Reilly, Comparison of first principles and semi-empirical models of the structural and electronic properties of $\text{Ge}_{1-x}\text{Sn}_x$ alloys, *Opt. Quantum Electron.* **51**, 314 (2019).
- [27] T. D. Eales, I. P. Marko, S. Schulz, E. O'Halloran, S. Ghetmiri, W. Du, Y. Zhou, S.-Q. Yu, J. Margetis, J. Tolle, E. P. O'Reilly, and S. J. Sweeney, $\text{Ge}_{1-x}\text{Sn}_x$ alloys: Consequences of band

- mixing effects for the evolution of the band gap Γ -character with Sn concentration, *Sci. Rep.* **9**, 14077 (2019).
- [28] S. Birner, T. Zibold, T. Andlauer, T. Kubis, M. Sabathil, A. Trellakis, and P. Vogl, nextnano: General purpose 3-D simulations, *IEEE Trans. Electron Devices* **54**, 2137 (2007).
- [29] A. Khaetskii, V. Golovach, and A. Kiefer, Revisiting the physical origin and nature of surface states in inverted-band semiconductors, *Phys. Rev. B* **105**, 035305 (2022).
- [30] I. Belopolski, S.-Y. Xu, N. Koirala, C. Liu, G. Bian, V. N. Strocov, G. Chang, M. Neupane, N. Alidoust, D. Sanchez, H. Zheng, M. Brahlek, V. Rogalev, T. Kim, N. C. Plumb, C. Chen, F. Bertran, P. L. Fèvre, A. Taleb-Ibrahimi, M.-C. Asensio *et al.*, A novel artificial condensed matter lattice and a new platform for one-dimensional topological phases, *Sci. Adv.* **3**, e1501692 (2017).
- [31] A. Giorgioni, S. Paleari, S. Cecchi, E. Vitiello, E. Grilli, G. Isella, W. Jantsch, M. Fanciulli, and F. Pezzoli, Strong confinement-induced engineering of the g factor and lifetime of conduction electron spins in Ge quantum wells, *Nat. Commun.* **7**, 13886 (2016).
- [32] S. De Cesari, A. Balocchi, E. Vitiello, P. Jahandar, E. Grilli, T. Amand, X. Marie, M. Myronov, and F. Pezzoli, Spin-coherent dynamics and carrier lifetime in strained $\text{Ge}_{1-x}\text{Sn}_x/\text{Ge}$ semiconductors on silicon, *Phys. Rev. B* **99**, 035202 (2019).
- [33] C.-T. Tai, P.-Y. Chiu, C.-Y. Liu, H.-S. Kao, C. T. Harris, T.-M. Lu, C.-T. Hsieh, S.-W. Chang, and J.-Y. Li, Strain effects on Rashba spin-orbit coupling of 2D hole gases in GeSn/Ge heterostructures, *Adv. Mater.* **33**, 2007862 (2021).
- [34] S. Assali, A. Attiaoui, P. D. Vecchio, S. Mukherjee, J. Nicolas, and O. Moutanabbir, A light-hole germanium quantum well on silicon, *Adv. Mater.* **34**, 2201192 (2022).